

# Influences of Device Architectures on Characteristics of Organic Light-Emitting Devices Incorporating Ambipolar Blue-Emitting Ter(9,9-diarylfluorenes)

Y.-T. Lin<sup>a</sup>, L.-Y. Chen<sup>a</sup>, Chung-Chih Wu<sup>a</sup>, K.-T. Wong<sup>b</sup>, R.-T. Chen<sup>b</sup>, Y.-Y. Chien<sup>b,a</sup>

<sup>a</sup> Dept. of Elec. Eng., Graduate Institute of Electro-optical Eng., and Graduate Institute of Electronics Eng., National Taiwan University, Taipei, Taiwan 10617, Republic of China

<sup>b</sup> Dept. of Chemistry, National Taiwan University, Taipei, Taiwan 10617, Republic of China

Email: [chungwu@cc.ee.ntu.edu.tw](mailto:chungwu@cc.ee.ntu.edu.tw)

**Abstract**— In this article, we report the studies of various device architectures of organic light-emitting devices (OLEDs) incorporating highly efficient blue-emitting and ambipolar carrier-transport ter(9,9-diarylfluorene)s, and their influences on device characteristics. The device structures investigated include single-layer devices and multilayer heterostructure devices employing the terfluorene as one functional layer. It is found that, although these terfluorenes are capable of bipolar carrier transport, rather poor device performance of single-layer devices in comparison with multilayer devices indicates that the heterostructure is still essential for balancing hole/electron injection and currents, for achieving high emission efficiencies, and for full utilization of high luminescence efficiency of these terfluorenes. With the heterostructure of hole-transport layer/terfluorene/electron-transport layer and careful choice of carrier-transport materials, effective hole and electron injection, confinement of carriers, and confinement of excitons in terfluorenes are achieved. As a consequence, a highly efficient (4.1% quantum efficiency), low-voltage (~2.5 V turn-on voltage), and color-saturated non-doped blue-emitting device is demonstrated. Such high electroluminescent efficiency is consistent with high photoluminescent quantum yields of these terfluorenes and is competitive with those of efficient doped blue OLEDs.

**KEYWORDS:** ambipolar carrier-transport, blue-emitting OLEDs, terfluorene, single-layer devices, heterostructure devices.

## I. INTRODUCTION

Organic light-emitting devices (OLEDs) have been the subjects of intense investigation in recent years due to their applications in displays and lighting [1]-[3]. In lighting applications, white-emitting devices are most desired, while in display applications the full-color capability is required. In all these applications, good blue-emitting materials and devices have been essential and therefore there have been continual efforts on exploring blue-emitting materials and devices with improved characteristics [4]-[9].

Among various blue-emitting materials reported [4]-[15], fluorene-based polymers or compounds have attracted wide interest in recent years as efficient blue emitters due to their high luminescence efficiency and flexibility in tuning various physical, optical and electrical properties through convenient substitution on C9 [10]-[15]. In our previous studies we have found ter(9,9-diarylfluorene)s (TDAF's) 1 and 2 (Fig. 1(a)) exhibit some intriguing properties promising for blue light-emitting devices [16],[17], such as the steric conformation of molecules induced with the peripheral aryl substituents on C9, high glass transition temperatures of >200 °C, high thin-film photoluminescence (PL) quantum yields of ~90% in pure blue, and electrochemical stability as indicated by both reversible oxidation and reduction. They form stable and homogeneous amorphous films with vacuum deposition, a basic

requirement for OLED applications. Furthermore, these compounds show unusual nondispersive ambipolar carrier-transport properties with high carrier mobilities of the order of  $10^{-3} \text{ cm}^2/(\text{V}\cdot\text{s})$  for both holes and electrons [17].

In this paper, we report the investigation of various device architectures employing the unique optical and electrical properties of these terfluorenes and the influences of device structures on device characteristics of OLEDs.

The article is organized as follows: in Sec. II, experimental methods for material/device preparation and characterization are described. In Sec. III, material properties and results of various device architectures using these ambipolar terfluorenes are presented in sequence. Finally, Sec. IV concludes results of this work.

## II. EXPERIMENT

### A. Material Preparation and Characterization

TDAF's investigated in this work were synthesized through the Suzuki coupling reaction of 2,7-diboronate ester of 9,9'-diarylfuorene and 2-bromo-9,9'-diarylfuorene in the presence of  $\text{Pd}(\text{PPh}_3)_4$  and  $\text{P}^t\text{Bu}_3$  catalysts with high yields (75-83%). Further details of synthesis and chemical analysis had been previously reported [16]. Synthesized TDAF's were subject to purification by temperature-gradient sublimation before use in subsequent analyses and device fabrication.

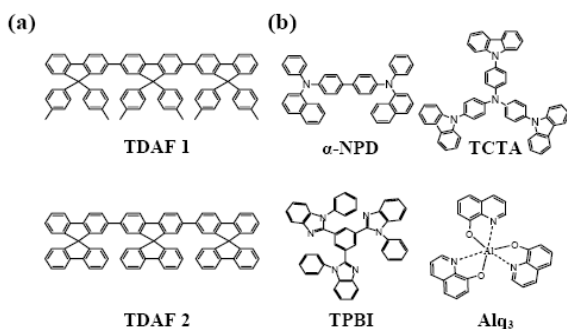


**Fig. 1** Chemical structures of various compounds used in this work. (a) TDAF 1 and 2. (b)  $\alpha$ -NPD, TCTA, Alq<sub>3</sub>, and TPBI.

Thin-film samples of organic compounds for optical characterization were prepared on quartz substrates by vacuum deposition in a high-vacuum chamber. The UV-visible

absorption spectra were measured on a Shimadzu UV-1601PC spectrophotometer. Photoluminescence (PL) spectra of thin-film samples were measured by pumping with a monochromatic light taken from a xenon arc lamp and by analyzing with a charge-coupled-device (CCD) spectrograph. The ionization potentials ( $I_p$ ) of organic thin films were measured using atmospheric low-energy photoelectron spectrometer Riken-Keiki AC-2 [18]-[21].

### B. Device Fabrication and Characterization

To study influences of device architectures on device characteristics, OLEDs incorporating the ambipolar TDAF's were fabricated and characterized. The devices were fabricated on glass substrates with the typical structure of multiple organic layers sandwiched between the bottom indium tin oxide (ITO) anode and the top metal cathode. Before use in device fabrication, the ITO-coated glass substrates were carefully cleaned. Cleaned ITO substrates were further treated with UV-ozone right before organic deposition [1]. The cathode used consists of a thin LiF layer as the electron injection layer and a thick Al layer as the metal electrode [22].

The stack of organic layers on ITO in sequence consists of a thin layer of conducting polymer polyethylene dioxythiophene/polystyrene sulphonate (PEDT:PSS, Bayer Corp.) and other functional layers of low molecular weight. The PEDT:PSS layer served as the hole-injection layer and was deposited by spin coating [23]. All other material layers in devices, including the metal cathode, were deposited by thermal evaporation in a multiple-source vacuum chamber with a base pressure of  $<10^{-6}$  Torr. The deposition rate of organic layers was kept at about 0.2 nm/s. The deposition system is equipped with a specially designed shutter and mask mechanism, so that a few devices with independently controlled structures can be fabricated in a single vacuum pump-down without breaking vacuum [24], permitting reliable side-by-side comparison of various 0.2 devices. The active area of the device is  $2 \times 2 \text{ mm}^2$ , as defined by the shadow mask for cathode deposition.

The current-voltage-brightness (I-V-L) characteristics of EL devices were measured using a source-measurement unit (SMU) and a Si photodiode calibrated with Photo Research PR-650 spectroradiometer. The EL spectra of OLEDs were taken with a calibrated CCD spectragraph.

### III. RESULTS AND DISCUSSIONS

#### A. Material Properties

Fig.1 shows the chemical structures of TDAF 1 and TDAF 2, and other compounds used in this study. The aromatic amines  $\alpha$ -naphthyl-phenyl-phenyl-biphenyl diamine ( $\alpha$ -NPD) and 4,4',4''-tri-(N-carbazolyl)-triphenylamine (TCTA) were used as the hole-transport layer (HTL) in some device structures [25],[26], while tris(8-hydroxyquinoline)aluminum ( $\text{Alq}_3$ ) and 2,2',2''-(1,3,5-benzenetriyl)tris[1-phenyl-1H-benzimidazole] (TPBI) were used as the electron-transport layer (ETL) in some device structures [1],[27].

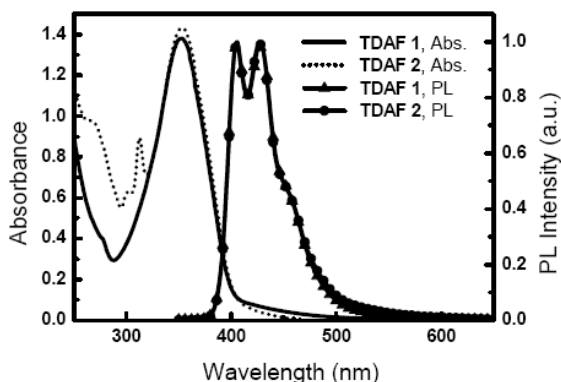


Fig. 2 Optical effective index for fundamental mode vs. active region thickness.

Fig. 2 shows the optical spectra of TDAF 1 and TDAF 2 in thin films. The absorption spectra of both terfluorenes exhibit an onset at  $\sim 405$  nm and a first peak at 351 nm. From the onset of absorption, the optical energy gaps ( $E_g$ ) of both TDAF's are estimated to be about 3.06 eV. PL of both TDAF's exhibits blue emission with two most prominent peaks around 405 nm and 430 nm. The PL quantum yields of both terfluorenes in thin films had been previously determined to be about 90% using an integrating sphere system [16], which

are among the highest for blue emitters in neat films [11], [12], [20], [28], [29].

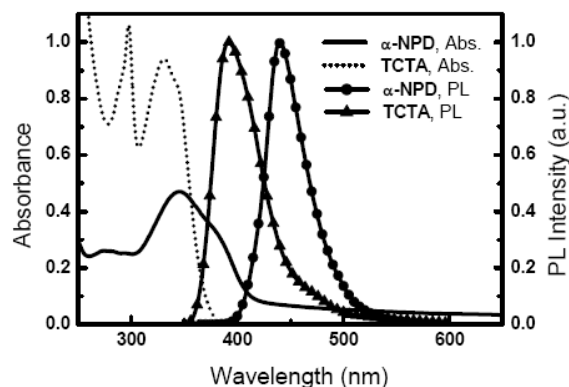


Fig. 3 Absorption and PL spectra for thin films of  $\alpha$ -NPD (100 nm) and TCTA (90 nm).

Fig. 3 shows the optical spectra of  $\alpha$ -NPD and TCTA in thin films. The absorption spectra of  $\alpha$ -NPD and TCTA exhibit onsets at  $\sim 415$  nm and  $\sim 375$  nm, respectively. From the onset of absorption, the optical energy gaps of  $\alpha$ -NPD and TCTA are estimated to be about 3.0 eV and 3.3 eV, respectively. PL of  $\alpha$ -NPD exhibits blue emission with the main peak around 440 nm, while that of TCTA shows UV emission with the main peak around 390 nm.

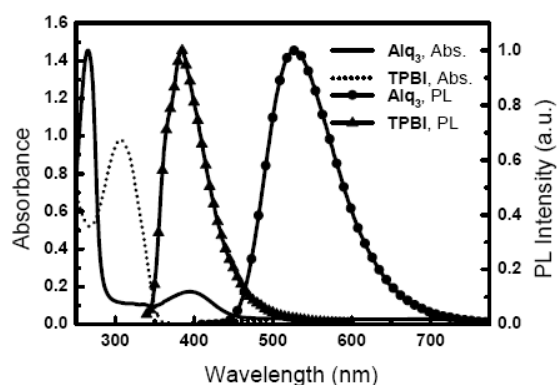


Fig. 4 Absorption and PL spectra for thin films of  $\text{Alq}_3$  (100 nm) and TPBI (100 nm).

Figure 4 shows the optical spectra of  $\text{Alq}_3$  and TPBI in thin films. The absorption spectra of  $\text{Alq}_3$  and TPBI exhibit onsets at  $\sim 450$  nm and  $\sim 360$  nm, respectively. From the onset of absorption, the optical energy gaps of  $\text{Alq}_3$  and TPBI are estimated to be about 2.8 eV and 3.4 eV, respectively. PL of  $\text{Alq}_3$  exhibits green emission with the main peak around 525 nm,

while that of TPBI shows UV emission with the main peak around 385 nm.

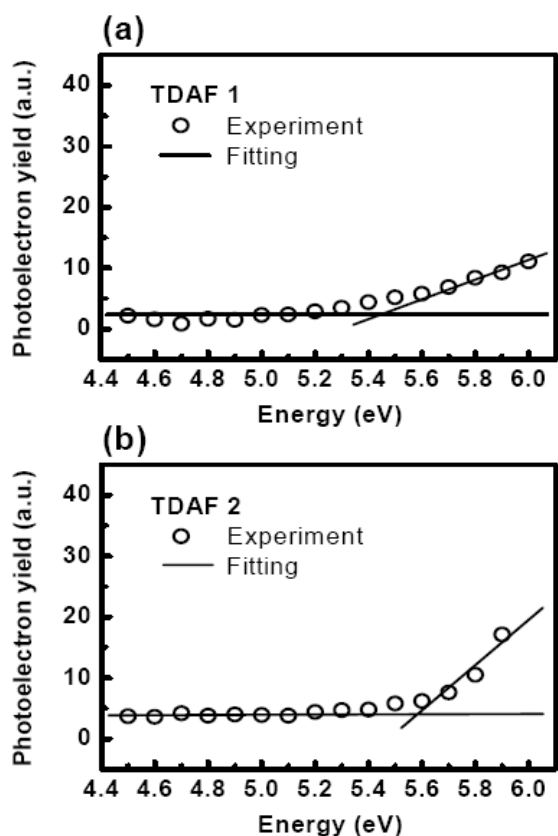


Fig. 5 Photoelectron spectra for thin films of (a) TDAF 1, and (b) TDAF 2.

Fig. 5 shows the photoelectron spectra of the TDAF's. From the onset of the photoelectron spectra, the ionization potentials ( $I_p$ ) of TDAF 1 and TDAF 2 are estimated to be  $\sim 5.4$ - $5.5$  eV and  $\sim 5.6$  eV, respectively. By subtracting the optical energy gaps from the measured thin-film ionization potentials, one obtains the electron affinities (EA) of  $\sim 2.34$ - $2.44$  eV and  $2.54$  eV for TDAF 1 and TDAF 2, respectively. Similarly, the ionization potentials of  $\alpha$ -NPD, TCTA, and Alq<sub>3</sub> were measured to be 5.3 eV, 5.5-5.6 eV, and 5.8 eV, respectively, and their electron affinities were estimated by subtracting the optical energy gaps from the measured thin-film ionization potentials (Table I). For TPBI, no photoemission onset was observed up to 6.2 eV in the photoelectron spectroscopy, which is the limit of the measurement range of the instrument used. It is indeed consistent with previously reported TPBI's  $I_p$  of all  $\geq 6.2$  eV [9], [30], [31]. All the energy levels along with other optical and

physical properties of various compounds are summarized in Table I.

**Table I** The energy levels and optical properties of various compounds in thin films

Compound	TDAF 1	TDAF 2	$\alpha$ -NPD	TCTA	Alq <sub>3</sub>	TPBI
$\lambda_{\text{max, abs}}^a$	350	350	345	300	395	305
$\lambda_{\text{onset, abs}}^b$	405	405	415	375	450	360
$\lambda_{\text{max, PL}}^c$	405, 430	405, 430	440	390	525	385
$E_g^d$	3.06	3.06	3.0	3.3	2.8	3.4
$I_p^e$	5.4~5.5	$\sim 5.6$	5.3	5.5~5.6	5.8	$\geq 6.2$
EA <sup>f</sup>	2.34~2.44	$\sim 2.54$	2.3	2.2~2.3	3.0	$\leq 2.8$

<sup>a</sup>First absorption peak (nm); <sup>b</sup>Absorption onset (nm); <sup>c</sup>Photoluminescence peak (nm); <sup>d</sup>Optical energy gap (eV); <sup>e</sup>Ionization potential (eV); <sup>f</sup>Electron affinity (eV)

## B. Single-Layer Device

Since the present terfluorene compounds are effective in transporting both holes and electrons, we first explored the device architecture comprising only a single layer of the TDAF sandwiched between a hole-injection contact and an electron-injection contact. The device structures used are: **Device A:** ITO/PEDT:PSS ( $\sim 30$  nm)/TDAF 1 (100 nm)/LiF (0.5 nm)/Al (150 nm), **Device B:** ITO/PEDT:PSS ( $\sim 30$  nm)/TDAF 2 (100 nm)/LiF (0.5 nm)/Al (150 nm).

Fig. 6 shows the spectral, current-voltage-brightness (I-V-L) and efficiency characteristics of the single-layer devices A and B. Both devices exhibit blue electroluminescence (EL) similar to PL of TDAF's (inset of Fig. 6(a)) and brightnesses up to 600-800 cd/m<sup>2</sup> at  $\sim 10$  V (Fig. 6(b)). The EL efficiencies of these single-layer devices are low, with a quantum efficiency of only  $\sim 0.15\%$  photon/electron (Fig. 6(c)). Considering the very high PL efficiencies of these materials, the low EL efficiencies are most possibly due to poor balance of hole and electron currents and/or poor confinement of carriers and excitons in the devices. Comparing the electrical characteristics of both devices (Fig. 6(a) and Fig. 6(b)), one finds that the device with TDAF 1 has slightly lower operating and turn-on voltages than the device with TDAF 2, where the turn-on voltage is defined as the voltage at which the emission starts to be detectable, i.e.  $\sim 10^{-3}$ - $10^{-4}$  cd/m<sup>2</sup>.

luminescence and low EL efficiencies [32]-[34].

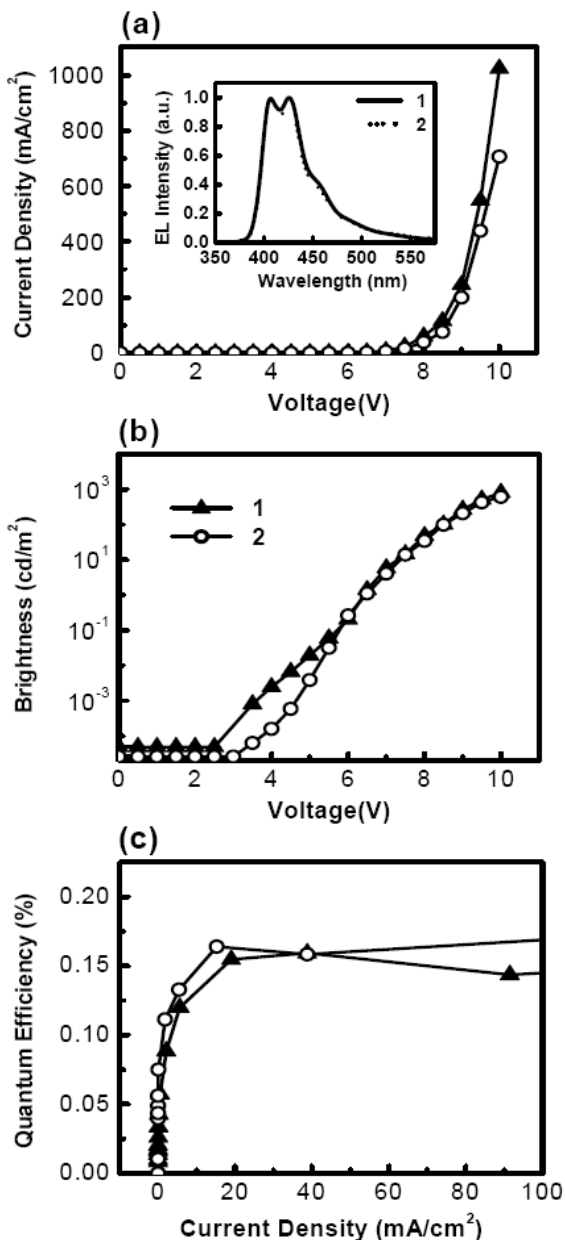


**Fig. 6** Device characteristics of ITO/PEDT:PSS (30 nm)/TDAF 1 or 2 (100 nm)/LiF (0.5 nm)/Al (150 nm): (a) I-V characteristics, (b) L-V characteristics, and (c) external quantum efficiency vs. current. Inset of (a): EL spectra of the devices.

In view of the fact that compound TDAF 1 has both lower  $I_p$  and EA than TDAF 2 (Table I) and , such results may suggest that in these single-layer devices, the device current is somewhat dominated by the hole current and the EL efficiency is more or less limited by injection of electrons. A further consequence of such unbalanced currents is that the carrier recombination may occur close to the cathode, leading to substantial quenching of

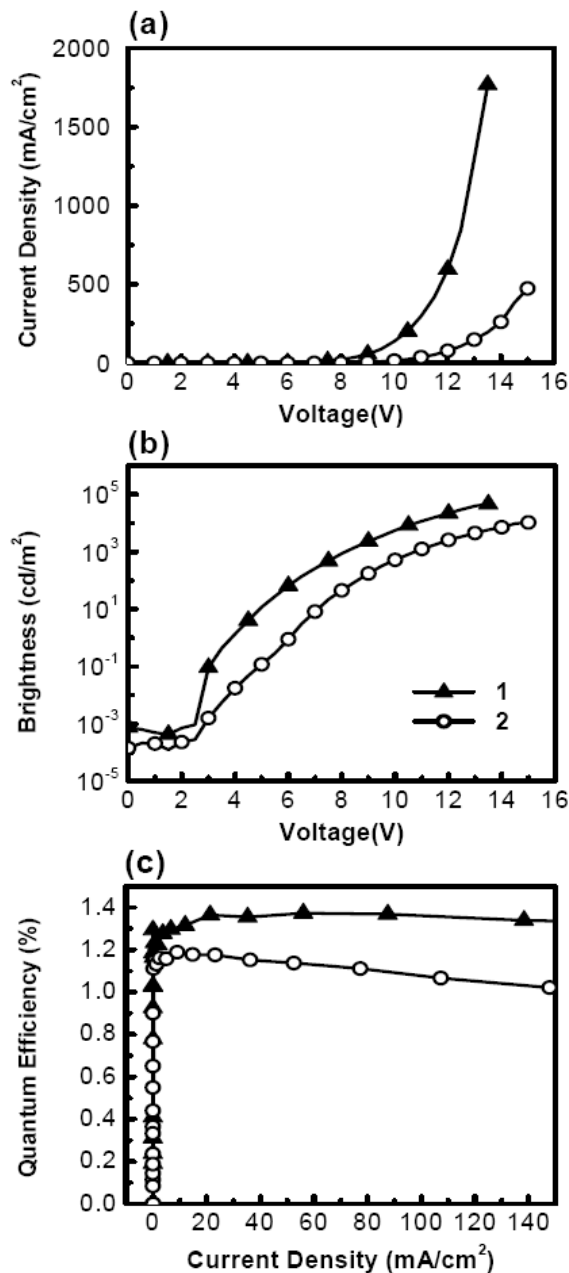


**Fig. 7** Device characteristics of ITO/PEDT:PSS (30 nm)/TDAF 1 or 2 (50 nm)/Alq<sub>3</sub> (50 nm)/LiF (0.5 nm)/Al (150 nm): (a) I-V characteristics, (b) L-V characteristics, and (c) external quantum efficiency vs. current. Inset of (a): EL spectra of the devices.

**C. Double-Layer Devices with Terfluorene as the Hole-Transport Layer**

Results of single-layer devices suggest that even though the present TDAF's possess ambipolar carrier-transport properties, heterostructures in devices may still be a

necessity to balance hole/electron injection and currents for enhancing device performance. More advanced heterostructure devices employing these TDAF's as the hole-transport layer in combination with another electron-transport layer with a better capability of electron injection, or employing these TDAF's as the electron-transport layer with another hole-transport layer, were then investigated. In this section, double-layer device structures using TDAF's as the hole-transport layer are first discussed. First, the frequently used electron-transport material Alq<sub>3</sub> was used to form the following device structures:

**Device C:** ITO/PEDT:PSS (~30 nm)/TDAF 1 (50 nm)/Alq<sub>3</sub> (50 nm)/LiF (0.5 nm)/Al (150 nm),

**Device D:** ITO/PEDT:PSS (~30 nm)/TDAF 2 (50 nm)/Alq<sub>3</sub> (50 nm)/LiF (0.5 nm)/Al (150 nm).

Fig. 7 shows the spectral, current-voltage-brightness and efficiency characteristics of double-layer devices C and D. Both devices exhibit green EL purely from Alq<sub>3</sub> (inset of Fig. 7(a)), indicating that injected electrons are effectively confined in Alq<sub>3</sub> presumably due to the substantial energy offset for electrons at the terfluorene/Alq<sub>3</sub> interface (EA in Table I) while holes can be injected into Alq<sub>3</sub> from the TDAF side. These devices exhibit EL quantum efficiencies of 1.2-1.4% (Fig. 7(c)), low turn-on voltage of ~2-2.5 V, and high EL brightnesses of ~46000 cd/m<sup>2</sup> (Device C, at ~13.5V) and 10560 cd/m<sup>2</sup> (Device D, at ~15 V) (Fig. 7(b)). These EL performances are comparable to conventional non-doped Alq<sub>3</sub>-based devices using arylamines as the hole-transport material [22], [24], [25], [35], [36]. Such results indicate that these terfluorenes function well as the hole-transport material in OLED applications. It is not too surprising since they have hole-transport mobilities similar to those of arylamine-based compounds [17], [37]. It is noteworthy that these terfluorenes have very high T<sub>g</sub>'s (>200 °C), which might give the OLED devices enhanced thermal stability [38].

Comparing the electrical characteristics of both devices, one finds that the device with TDAF 1 has lower voltage and slightly higher

efficiency than the device with TDAF 2. This is consistent with the fact that compound TDAF 1 has a lower I<sub>p</sub> than compound TDAF 2 (Table I), and therefore that hole injection from the anode might be more efficient with compound TDAF 1.

Using Alq<sub>3</sub> as the electron-transport material, the device EL efficiency is greatly enhanced presumably due to improved electron injection. The emission, however, is from Alq<sub>3</sub>, instead of from the desired TDAF's. To attain this object, the electron-transport material TPBI, which has a larger I<sub>p</sub>, a larger energy gap and a smaller EA than Alq<sub>3</sub> (Table I), was adopted with the aim of confining holes in terfluorenes while passing electrons. The device structures investigated are as follows:

**Device E:** ITO/PEDT:PSS (~30 nm)/TDAF 1 (50 nm)/TPBI (50 nm)/LiF (0.5 nm)/Al (150 nm),

**Device F:** ITO/PEDT:PSS (~30 nm)/TDAF 2 (50 nm)/TPBI (50 nm)/LiF (0.5 nm)/Al (150 nm),

**Device G:** ITO/PEDT:PSS (~30 nm)/TDAF 1 (50 nm)/TPBI (37 nm)/LiF (0.5 nm)/Al (150 nm),

**Device H:** ITO/PEDT:PSS (~30 nm)/TDAF 2 (50 nm)/TPBI (37 nm)/LiF (0.5 nm)/Al (150 nm).

The last two devices (G, H) are similar to the first two devices (E, F) except for the difference in the thickness of TPBI.

Figure 8 shows the spectral, current-voltage-brightness and efficiency characteristics of the double-layer devices E-H. All devices exhibit blue EL purely from terfluorenes (Fig. 8(a)), indicating that injected holes are confined in TDAF's while electrons are effectively passed by TPBI to TDAF's for recombination with holes there.

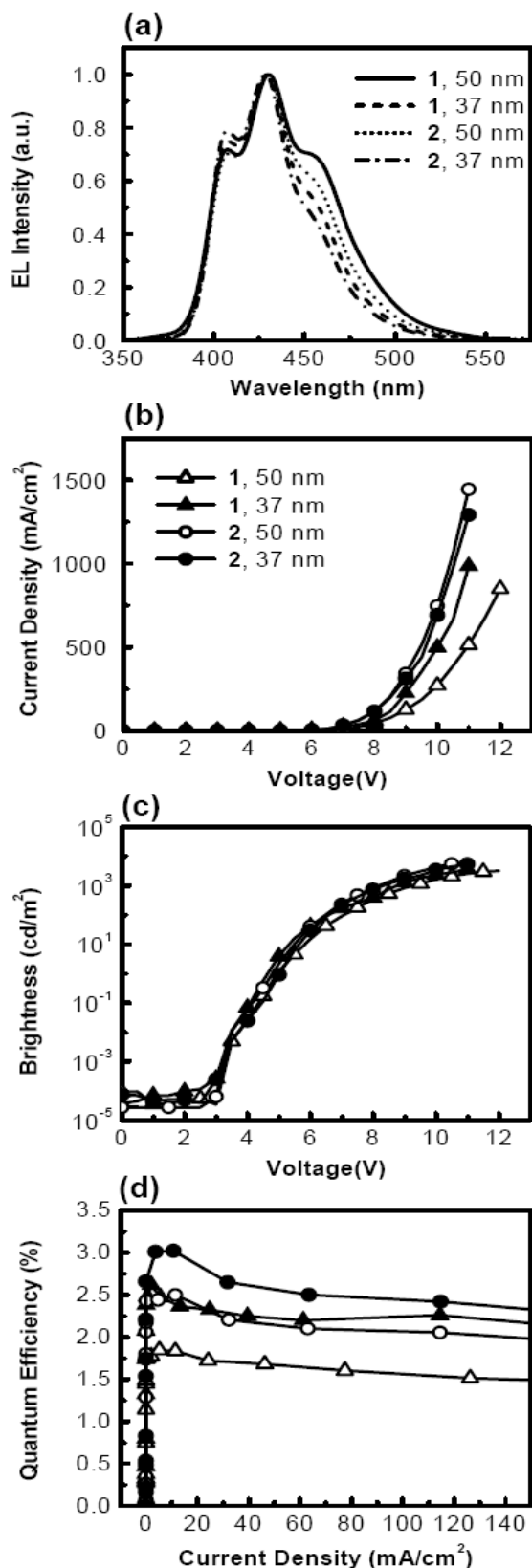


**Fig. 8** Device characteristics of ITO/PEDT:PSS (30 nm)/TDAF 1 or 2 (50 nm)/TPBI (37 nm or 50 nm)/LiF (0.5 nm)/Al (150 nm): (a) EL spectra of the devices, (b) I-V characteristics, (c) L-V characteristics, and (d) external quantum efficiency vs. current.

In comparison to the single-layer devices discussed earlier, these devices exhibit substantially enhanced blue EL quantum efficiencies of 1.7-3.0%, depending on the TDAF used and the TPBI thickness (Fig. 8(d)). In view of the fact that these blue-emitting devices are non-doped, the EL efficiencies observed for the present devices are rather high for blue OLEDs [4]-[10], [20], [31]. Such results indicate the effectiveness of TPBI on enhancing electron injection into TDAF's and balancing hole/electron currents of devices. As a consequence, all these blue-emitting devices exhibit rather low turn-on voltages of  $\sim 3$  V and substantially enhanced blue emission. Brightnesses of a few thousand of  $\text{cd/m}^2$  (3200  $\text{cd/m}^2$  at 12 V for device E, 6370  $\text{cd/m}^2$  at 11 V for device F, 3655  $\text{cd/m}^2$  at 11 V for device G, 5380  $\text{cd/m}^2$  at 11 V for device H) are obtained in these devices (Fig. 8(c)).

It is noteworthy that in this set of devices, the devices using TDAF 1 as the hole-transport material have higher voltage than the devices using TDAF 2 as the hole-transport material (Fig. 8(b)), in contrast to the observations in preceding devices. This may indicate that in these devices the current flow is somewhat controlled by injection of electrons from TPBI to terfluorenes, since one may expect the energy offset between TPBI and TDAF 1 be larger than that between TPBI and TDAF 2 (Table I).

It is also noticed that the EL spectra and EL efficiencies are subtly affected by the layer thicknesses of devices, in particular the thickness of TPBI in the present cases. Devices with 37 nm TPBI show higher EL efficiencies (2.5% for Device G, 3% for Device H) than devices with 50 nm TPBI (1.75% for Device E, 2.5% for Device F). Further, there is noticeable difference in the spectral shape between PL of TDAF's and EL of these devices, and between EL of different device structures (Fig. 8(a)). For example, devices with thinner (37 nm) TPBI show narrower EL spectra than devices with thicker TPBI (50 nm). These effects are attributed to the difference in optical environments for PL and EL, and the cavity effects of OLED devices [39]-[41]. In EL, the strong reflection of the metal cathode induces stronger wavelength-dependent interference

and cavity effects, resulting in wavelength-dependent and location-dependent coupling-out efficiency of internal exciton emission. Therefore, EL spectra and efficiencies are more sensitive to the position and the distribution of emitting excitons relative to the metal mirror and the total cavity length [39]-[41]. Similar variations of EL spectra of TDAF's can be repeatedly found in various device architectures when comparing EL spectra of all devices in this paper. It has been shown that careful adjustment of layer thickness is essential for optimizing color and efficiency of OLED devices [39]-[41].

#### D. Double-Layer Devices with Terfluorene as the Electron-Transport Layer

On the other hand, since these TDAF's also possess electron-transport capability comparable to their hole-transport capability, devices employing them as the electron-transport layer were also investigated. Initially, the frequently used hole-transport material  $\alpha$ -NPD was used in combination with TDAF's to form the following device structures:

**Device I:** ITO/PEDT:PSS (~30 nm)/ $\alpha$ -NPD (50 nm)/TDAF 1 (50 nm)/LiF (0.5 nm)/Al (150 nm),

**Device J:** ITO/PEDT:PSS (~30 nm)/ $\alpha$ -NPD (50 nm)/TDAF 2 (50 nm)/LiF (0.5 nm)/Al (150 nm).

Figure 9 shows the spectral, current-voltage-brightness and efficiency characteristics of the double-layer devices I and J. Comparing device EL spectra (inset of Fig. 9(a)) with PL spectra of TDAF's and  $\alpha$ -NPD (Fig. 2 and Fig. 3), one concludes that both devices exhibit blue EL purely from  $\alpha$ -NPD with EL quantum efficiencies of 0.7-0.9% (Fig. 9(c)) and brightness up to  $\sim 2000$  cd/m<sup>2</sup>. These device characteristics indicate that injected holes are mostly confined within  $\alpha$ -NPD while electrons are passed to  $\alpha$ -NPD for recombination. According to these results, it appears that these TDAF's function as a hole-blocking and electron-transport layer for  $\alpha$ -NPD.

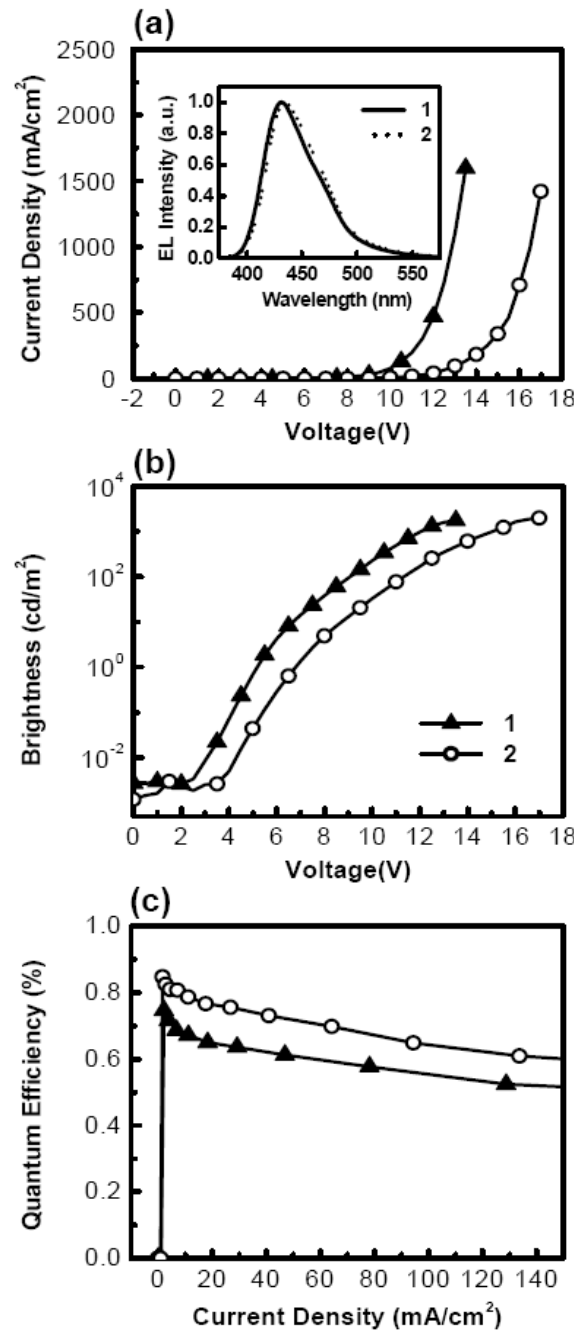


**Fig. 9** Device characteristics of ITO/PEDT:PSS (30 nm)/ $\alpha$ -NPD (50 nm)/TDAF 1 or 2 (50 nm)/LiF (0.5 nm)/Al (150 nm): (a) I-V characteristics, (b) L-V characteristics, and (c) external quantum efficiency vs. current. Inset of (a): EL spectra of the devices.

To attain injection of holes into and confinement of electrons within the TDAF's, a hole-transport material, TCTA, which has a larger  $I_p$ , a larger energy gap, and a smaller EA than  $\alpha$ -NPD, was then tested as a hole-transport layer for the TDAF's. The device structures investigated are as follows:



**Device K:** ITO/PEDT:PSS (~30 nm)/TCTA (50 nm)/TDAF 1 (50 nm)/LiF (0.5 nm)/Al (150 nm),

**Device L:** ITO/PEDT:PSS (~30 nm)/TCTA (50 nm)/TDAF 2 (50 nm)/LiF (0.5 nm)/Al (150 nm).

Figure 10 shows the spectral, current-voltage-brightness and efficiency characteristics of the double-layer devices K and L. Both devices exhibit blue EL purely from TDAF's (inset of Fig. 10(a)), indicating that injected electrons are effectively confined in TDAF's while TCTA passes holes to TDAF's for recombination with electrons there. Both devices exhibit turn-on voltage of ~3V, and brightnesses up to 2000-3000 cd/m<sup>2</sup> (2100 cd/m<sup>2</sup> at 11V for device K, 2415 cd/m<sup>2</sup> at 10.5 V for device L) are obtained (Fig. 10(b)).

The EL quantum efficiencies of 0.6%-0.8% for these devices (Fig. 10(c)) are substantially enhanced in comparison with preceding single-layer devices, indicating effectiveness of TCTA on confining electrons in TDAF's and balancing hole/electron currents. Although one may not expect such effective electron blocking due to lack of significant difference in EA levels of TCTA and TDAF's, the capability of TCTA in blocking electrons may originate from the fact that it transports holes only and hardly transports electrons [37]. As revealed in previous studies [42], in addition to heterostructures containing energy offsets, heterostructures that contain large carrier-mobility offset (i.e. difference) are equally effective in confining carriers and in controlling distribution of carriers. The EL efficiencies of the TCTA/TDAF devices, however, are substantially lower than the TDAF/TPBI double-layer devices. Such difference may be due to the fact that even with the TCTA/TDAF heterostructure, the electron injection from the cathode into TDAF's may still be an issue to the device efficiency.

#### E. Triple-Layer Device with Terfluorene as the Emitting Layer

In the preceding TCTA/TDAF and TDAF/TPBI double-layer heterostructure devices, one type of the carriers (electrons in the TCTA/TDAF structure, or holes in the

TDAF/TPBI structure) is effectively confined in TDAF due to the existence of energy offset or carrier-mobility offset at the heterojunction. However, the other type of the carriers (holes in the TCTA/TDAF structure, or electrons in the TDAF/TPBI structure), when injected into the TDAF, may travel deep into TDAF before recombination and may not be effectively confined near the junction due to its ambipolar carrier-transport nature. The consequences may be manifold. First, some carriers may travel through without recombination. Second, the recombination zone may be broadly distributed in the TDAF, having a substantial portion of the recombination zone in the proximity of the electrodes and subject to electrode quenching of luminescence. All these situations, if occurring, are detrimental to emission efficiency of devices. As an indication, the observed EL quantum efficiencies for the preceding double-layer devices (0.6-0.8% for TCTA/TDAF devices and 1.7-3% for TDAF/TPBI devices) are clearly lower than one can expect from the very high thin-film PL quantum yields of ~90 % for these TDAF's, assuming balanced hole/electron injection/transport and ideal carrier recombination. Therefore, there is room for further improvement of device performance through more effective confinement of carriers and excitons.

To more effectively confine both carriers in the TDAF's and to further enhance device EL efficiencies, a more advanced device structure with the TCTA/TDAF/TPBI double heterostructure was investigated. Such structure makes use of the capability of TCTA in blocking electrons and the capability of TPBI in blocking holes while having appropriate carrier-transport properties. In addition, TCTA and TPBI have the further advantage of confining excitons within terfluorenes since both TCTA and TPBI have larger energy gaps (3.3 eV for TCTA and 3.4 eV for TPBI) than the present TDAF's (3.06 eV).

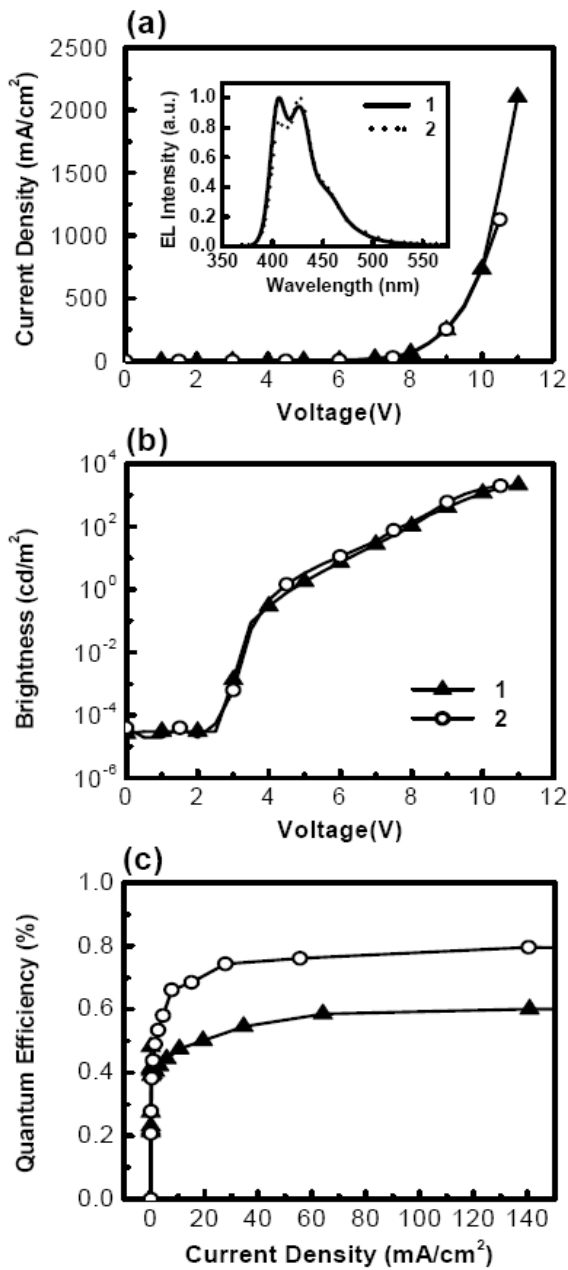


**Fig. 10** Device characteristics of ITO/PEDT:PSS (30 nm)/TCTA (50 nm)/TDAF 1 or 2 (50 nm)/ LiF (0.5 nm)/Al (150 nm): (a) I-V characteristics, (b) L-V characteristics, and (c) external quantum efficiency vs. current. Inset of (a): EL spectra of the devices.

Such exciton confinement could hinder excitons from diffusing towards electrodes or transferring energy to neighboring charge-transport layers with lower-energy emission and/or less efficient luminescence, giving further benefits to device efficiency and color purity. The device structures investigated are as follows:

**Device M:** ITO/PEDT:PSS (~30 nm)/TCTA (40 nm)/TDAF 1 (30 nm)/TPBI (30 nm)/LiF (0.5 nm)/Al (150 nm),

**Device N:** ITO/PEDT:PSS (~30 nm)/TCTA (40 nm)/TDAF 2 (30 nm)/TPBI (30 nm)/LiF (0.5 nm)/Al (150 nm).

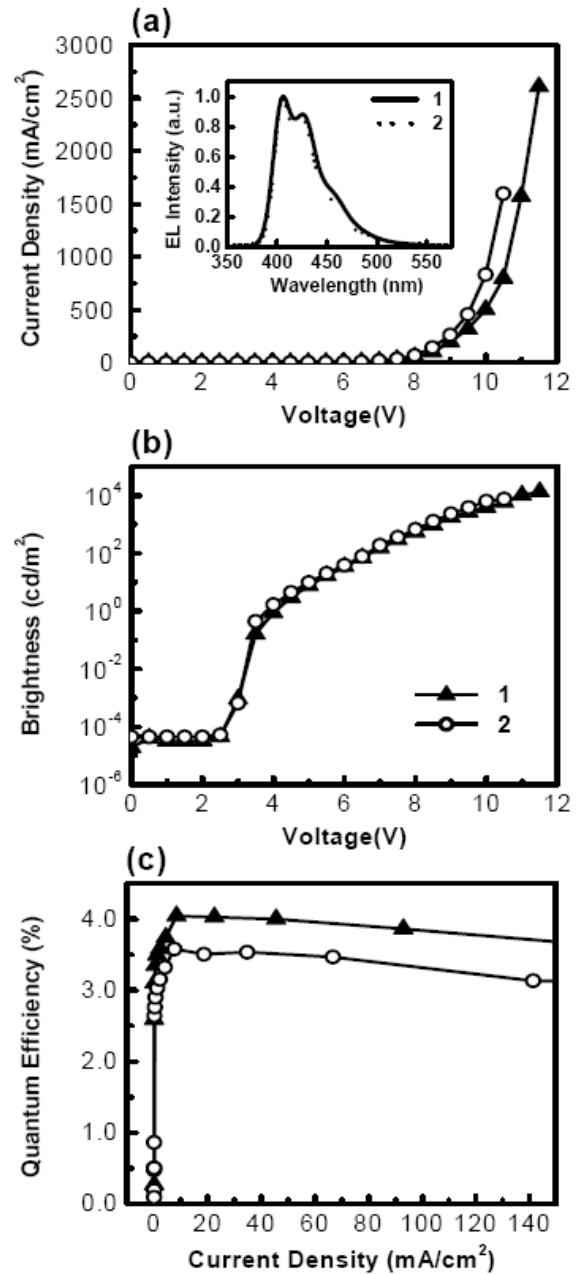


**Fig. 11** Device characteristics of ITO/PEDT:PSS (30 nm)/TCTA (40nm)/TDAF 1 or 2 (30 nm)/TPBI (30 nm)/ LiF (0.5 nm)/Al (150 nm): (a) I-V characteristics, (b) L-V characteristics, and (c) external quantum efficiency vs. current. Inset of (a): EL spectra of the devices.

Figure 11 shows the spectral, current-voltage-brightness and efficiency characteristics of the triple-layer devices M and

N. Both devices exhibit blue EL purely from TDAF's (inset of Fig. 11(a)). These devices exhibit the best blue EL quantum efficiencies of 3.6-4.1% (4.1% for device M, 3.6% for device N, Fig. 11(c)) among all of the blue-emitting devices discussed in this article. Such high EL efficiencies are more consistent with the high PL quantum yields of TDAF's and indicate the effectiveness of the present double heterostructure on better confinement of carriers and excitons. High brightnesses of  $\sim 14000$  and  $\sim 8000$   $\text{cd/m}^2$  are obtained for devices M (at 11.5 V) and N (at 10.5 V) (Fig. 11(b)), respectively, an apparent enhancement relative to those of double-layer devices. In view of the fact that these blue-emitting devices are non-doped, the EL efficiencies are very high for pure blue OLEDs, even competitive with the best of doped blue OLEDs [4], [7], [9], [20]. Furthermore, these devices exhibit rather low turn-on voltage of  $\sim 2.5\text{V}$  (Fig. 11(b)). Such low turn-on voltage is also rare for blue OLEDs, which in nature incorporate large-gap materials (at least the emitting material) in the device structure and usually render larger difficulty in achieving low voltage [7], [9]. In general, all devices with emission from TDAF's in the article exhibit very pure and saturated blue emission. As an instance, EL of devices M and device N have 1931 CIE coordinates of (0.158, 0.041) and (0.160, 0.044), respectively. As shown in the 1931 CIE chromaticity diagram of Fig. 12, these coordinates are very close to the NTSC (National Television Standards Committee) blue standard.

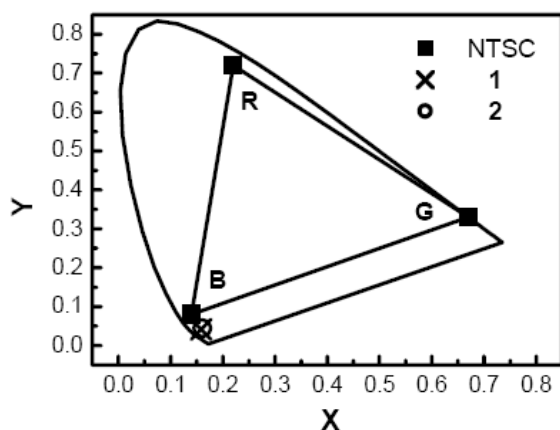


**Fig. 12** 1931 CIE coordinates of EL of devices M (TDAF 1) and N (TDAF 2), along with the NTSC standards.

The first demonstration of double-heterostructure OLEDs that provides effective confinement on both types of carriers and excitons was reported by Adachi et al. for green OLEDs [43]. The application of such device configurations to blue OLEDs, however, is more difficult in general mainly because of the difficulty in finding appropriate carrier-transport materials to meet many requirements, such as relatively large energy gaps (e.g.  $>3$  eV) for exciton confinement, energy levels matching relatively larger  $I_p$  and smaller EA of blue-emitting materials for carrier injection, and yet appropriate carrier-transport properties or energy levels for blocking the other type of carriers. For instance, employing the widely used electron-transport material  $\text{Alq}_3$  to blue OLEDs often leads to partial emission from  $\text{Alq}_3$  (green emission) and deterioration of color purity of blue EL, mainly due to lack of effective exciton confinement and hole blocking [9], [44]. The TCTA/TDAF/TPBI structure reported here therefore represents one of the rare cases of double heterostructure blue OLEDs that possess effective confinement of both types of carriers and emitting excitons in the blue-emitting layer.

#### F. Four-Layer Device with Terfluorene as the Emitting Layer

In the preceding TCTA/TDAF/TPBI heterostructure, the use of TCTA as the hole-transport layer provides for hole injection into and electron confinement within TDAF, substantially enhancing EL efficiency. TCTA, however, has slightly higher  $I_p$  than other widely used hole-transport materials, such as  $\alpha$ -NPD, which may affect hole injection from the anode and the operation voltage. To test whether one can further enhance device performance, an intermediate hole-transport layer with a smaller  $I_p$ ,  $\alpha$ -NPD, is inserted between the anode and TCTA to form the following device structure:

**Device O:** ITO/PEDT:PSS ( $\sim 30$  nm)/ $\alpha$ -NPD (20 nm)/TCTA (20 nm)/TDAF 1 (30 nm)/TPBI (30 nm)/LiF (0.5 nm)/Al (150 nm).

Fig. 13 compares the spectral, current-voltage-brightness and efficiency characteristics of devices M and O. From Fig.

13(a) and 13(b), one sees that inserting  $\alpha$ -NPD between the anode and TCTA indeed reduces the device operation voltage, confirming the effectiveness of multiple hole-transport layers in improving hole-injection and transport.

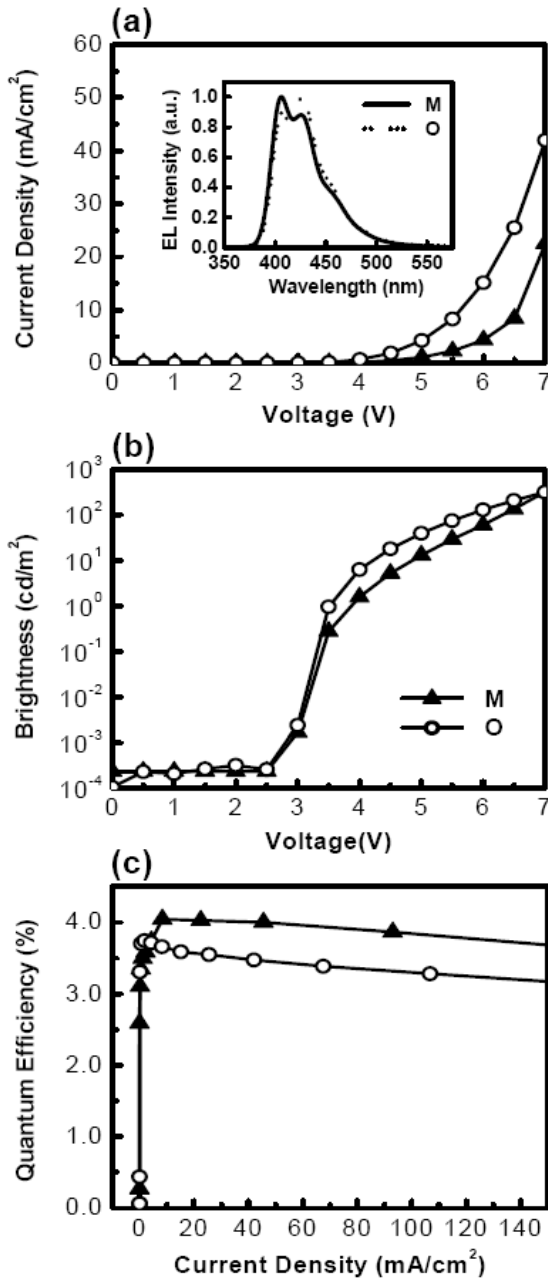


**Fig. 13** Comparison of device characteristics of Device M: ITO/PEDT:PSS (30 nm)/TCTA (40 nm)/TDAF 1 (30 nm)/TPBI (30 nm)/ LiF (0.5 nm)/Al (150 nm), and Device O: ITO/PEDT:PSS (30 nm)/ $\alpha$ -NPD (20 nm)/TCTA (20 nm)/TDAF 1 (30 nm)/TPBI (30 nm)/ LiF (0.5 nm)/Al (150 nm): (a) I-V characteristics, (b) L-V characteristics, and (c) external quantum efficiency vs. current. Inset of (a): EL spectra of the devices.

Device O however also shows a slightly reduced EL efficiency (3.8%) than that of device M (4.1%) (Fig. 13(c)). Such slight difference may result from optical absorption loss due to the overlap of TDAF's emission spectrum and  $\alpha$ -NPD's absorption spectrum. Comparing EL spectra of devices M and O (inset of Fig. 13(a)), the lower intensity at shorter wavelengths in the EL spectrum of device O may be regarded as an indication of such absorption loss.

#### IV. CONCLUSION

In summary, we report the influences of device architectures on device characteristics of OLEDs incorporating highly efficient blue-emitting and ambipolar carrier-transport ter(9,9-diarylfluorene)s. In consideration of their ambipolar carrier-transport nature, device architectures employing only a single layer of terfluorene between the injection electrodes, employing the terfluorene as the hole-transport layer or the electron-transport layer in double-layer heterostructure devices, or employing the terfluorene as the ambipolar emitting layer sandwiched between a hole-transport layer and an electron-transport layer are investigated. It is found that, although these terfluorenes are capable of bipolar carrier transport, rather poor device performance of single-layer devices in comparison with multilayer devices indicates the heterostructure is still essential for balancing hole/electron injection and currents, for achieving high EL efficiencies and for full utilization of high luminescence efficiency of these terfluorenes. However, it is found that there is difficulty in achieving hole injection into these terfluorenes using the conventional hole-transport material such as  $\alpha$ -NPD. Similarly, there is difficulty in achieving electron injection into the terfluorenes using the conventional electron-transport material Alq<sub>3</sub>. Such difficulties are removed by using a hole-transport material TCTA with a larger  $I_p$ , a smaller EA and a larger energy gap than  $\alpha$ -NPD, and an electron-transport material TPBI with a smaller EA, a larger  $I_p$  and a larger energy gap than Alq<sub>3</sub>. Finally, using the TCTA/terfluorene/TPBI double heterostructure results in a highly efficient (4.1% quantum efficiency), low-voltage ( $\sim 2.5$  V turn-on

voltage) and color-saturated non-doped blue-emitting device. Such high EL efficiencies are consistent with high PL quantum yields of these terfluorenes and are competitive with those of efficient doped blue OLEDs. Such enhancements are attributed to effective hole and electron injection, confinement of carriers, and confinement of excitons in terfluorenes with such double heterstructures.

#### ACKNOWLEDGMENT

This work was supported in part by National Science Council and Ministry of Education of the Republic of China.

#### REFERENCES

- [1] C. W. Tang and S. A. VanSlyke, *Appl. Phys. Lett.* 51, 913 (1987).
- [2] C.W. Tang, S.A. VanSlyke and C.H. Chen, *J. Appl. Phys.* 65, 3610 (1989).
- [3] F. Steuber, J. Staudigel, M. Stössel, J. Simmerer, A. Winnacker, H. Spreitzer, F. Weissörtel and J. Salbeck, *Adv. Mater.* 12, 130 (2000).
- [4] J. Shi, and C. W. Tang, *Appl. Phys. Lett.* 80, 3201 (2002).
- [5] Y.-H. Kim, D.-C. Shin, S.-H. Kim, C.-H. Ko, H.-S. Yu, Y.-S. Chae, and S.-K. Kwon, *Adv. Mater.* 13, 1690.
- [6] L.-H. Chan, H.-C. Yeh, and C.-T. Chen, *Adv. Mater.* 13, 1637 (2001).
- [7] C. Hosokawa, H. Higashi, H. Nakamura, and T. Kusumoto, *Appl. Phys. Lett.* 67, 3853 (1995).
- [8] Y. Kijima, N. Asai, and S.-I. Tamura, *Jpn. J. Appl. Phys.* 38, part 1, 5274 (1999).
- [9] Y. Li, M. K. Fung, Z. Xie, S.-T. Lee, L.-S. Hung, and J. Shi, *Adv. Mater.* 14, 1317 (2002).
- [10] K.-H. Weinfurter, F. Weissortel, G. Harmgarth, and J. Salbeck, *Proc. SPIE-Int. Soc. Opt. Eng.* 3476, 40 (1998)
- [11] D. Katsis, Y. H. Geng, J. J. Ou, S. W. Culligan, A. Trajkovska, S. H. Chen, and L. J. Rothberg, *Chem. Mater.* 14, 1332 (2002).
- [12] Y. Geng, D. Katsis, S. W. Culligan, J. J. Ou, S. H. Chen, and L. J. Rothberg, *Chem. Mater.* 14, 463 (2002).
- [13] M. Redecker, D. D. C. Bradley, M. Inbasekaran, and E. P. Woo, *Appl. Phys. Lett.* 73, 1565 (1998).
- [14] M. Belletête, M. Ranger, S. Beaupré, M. Leclerc, and G. Durocher, *Chem. Phys. Lett.* 316, 101 (2000).
- [15] S. Setayesh, A. C. Grimsdale, T. Weil, V. Enkelmann, K. Müllen, F. Meghdadi, E. J. W. List, G. Leising, *J. Am. Chem. Soc.* 123, 946 (2001).
- [16] K.-T. Wong; Y.-Y. Chien; R.-T. Chen; C.-F. Wang; Y.-T. Lin; H.-H. Chiang; P.-Y. Hsieh; C.-C. Wu; C. H. Chou; Y. O. Su; G.-H. Lee; and S.-M. Peng, *J. Am. Chem. Soc.* 124, 11576 (2002).
- [17] C.-C. Wu, T.-L. Liu, W.-Y. Hung, Y.-T. Lin, K.-T. Wong, R.-T. Chen, Y.-M. Chen, and Y.-Y. Chien, *J. Am. Chem. Soc.* 125, 3710 (2003).
- [18] T. Sano, Y. Hamada and K. Shibata, *IEEE J. Selected Topics in Quantum Electronics* 4, 34 (1998).
- [19] H. Kirihata, and M. Uda, *Rev. Sci. Instrum.* 52, 68 (1981).
- [20] C.-C. Wu, Y.-T. Lin, H.-H. Chiang, T.-Y. Cho, C.-W. Chen, K.-T. Wong, Y.-L. Liao, G.-H. Lee, and S.-M. Peng, *Appl. Phys. Lett.* 81, 577 (2002).
- [21] C.-C. Wu, W.-Y. Hung, T.-L. Liu, L.-Z. Zhang, and T.-Y. Luh, *J. Appl. Phys.* 93, 5465 (2003).
- [22] L. S. Hung, C. W. Tang, and M. G. Mason, *Appl. Phys. Lett.* 70, 152 (1997).
- [23] A. Elscher, F. Bruder, H.-W. Heuer, F. Jonas, A. Karbach, S. Kirchmeyer, S. Thurm, and R. Wehrmann, *Synth. Met.* 111, 139 (2000).
- [24] C.-W. Chen, T.-Y. Cho, C.-C. Wu, H.-L. Yu, and T.-Y. Luh, *Appl. Phys. Lett.* 81, 1570 (2002).

- [25] J. Shi and C. W. Tang, *Appl. Phys. Lett.* 70, 1665 (1997).
- [26] Y. Kuwabara, H. Ogawa, H. Inada, N. Noma, and Y. Shirota, *Adv. Mater.* 6, 677 (1994).
- [27] J. Shi, C. W. Tang, and C. H. Chen, U. S. Patent No. 5,646,948 (1997).
- [28] J. Salbeck, N. Yu, J. Bauer, F. Weissörtel, and H. Bestgen, *Synth. Met.* 91, 209 (1997).
- [29] M. R. Robison, S. Wang, G. C. Bazan, and Y. Cao, *Adv. Mater.* 12, 1701 (2000).
- [30] Z. Gao, C. S. Lee, I. Bello, S. T. Lee, R.-M. Chen, T.-Y. Luh, J. Shi, and C. W. Tang, *Appl. Phys. Lett.* 74, 865 (1999).
- [31] Y. T. Tao, E. Balasubramaniam, A. Danel, and P. Tomasik, *Appl. Phys. Lett.* 77, 1575 (2000).
- [32] V. Choong, Y. Park, Y. Gao, T. Wehrmeister, K. Müllen, B. R. Hsieh, and C. W. Tang, *Appl. Phys. Lett.* 69, 1492 (1996).
- [33] U. Lemmer, S. Karg, M. Scheidler, M. Deussen, W. Ries, B. Cleve, P. Thomas, H. Bässler, M. Schwoerer, and E. O. Göbel, *Synth. Met.* 67, 169 (1994).
- [34] R. Kersting, U. Lemmer, M. Deussen, H. J. Bakker, R. F. Mahrt, H. Kurz, V. I. Arkhipov, H. Bässler, and E. O. Göbel, *Phys. Rev. Lett.* 73, 1440 (1994).
- [35] J. Kido, *Appl. Phys. Lett.* 73, 2866 (1998).
- [36] T. Wakimoto, Y. Fukuda, K. Nagayama, A. Yokoi, H. Nakada, and M. Tsuchida, *IEEE. Trans. Electron Devices* 44, 1245 (1997).
- [37] Y. Shirota, *J. Mater. Chem.* 10, 1 (2000).
- [38] S. Tokito, H. Tanaka, K. Noda, A. Okada, and Y. Taga, *Appl. Phys. Lett.* 70, 1929 (1997).
- [39] V. Bulovic, V. V. Khalfin, G. Gu, P. E. Burrows, D. Z. Garbuzov, and S. R. Forrest, *Phys. Rev. B* 58, 3730 (1996).
- [40] W. M. V. Wan, N. C. Greenham, and R. H. Friend, *J. Appl. Phys.* 87, 2542 (2000).
- [41] S. K. So, W. K. Choi, L. M. Leung, and K. Neyts, *Appl. Phys. Lett.* 74, 1939 (1999).
- [42] B. K. Crone, P. S. Davids, I. H. Campbell, and D. L. Smith, *Appl. Phys. Lett.* 87, 1974 (2000).
- [43] C. Adachi, T. Tsutsui, and S. Saito, *Appl. Phys. Lett.* 57, 531 (1990).
- [44] L.-H. Chan, R.-H. Lee, C.-F. Hsieh, H.-C. Yeh, and C.-T. Chen, *J. Am. Chem. Soc.* 124, 6469 (2002).